Interdecadal Changes in the Relationship between Interannual Variations of Spring North Atlantic SST and Eurasian Surface Air Temperature

SHANGFENG CHEN

Center for Monsoon System Research, Institute of Atmospheric Physics, Chinese Academy of Sciences, Beijing, China

RENGUANG WU

Center for Monsoon System Research, and State Key Laboratory of Numerical Modeling for Atmospheric Sciences and Geophysical Fluid Dynamics, Institute of Atmospheric Physics, Chinese Academy of Sciences, Beijing, China

(Manuscript received 26 June 2016, in final form 12 January 2017)

ABSTRACT

This study investigates interdecadal changes in the relationship between interannual variations of boreal spring sea surface temperature (SST) in the North Atlantic and surface air temperature (SAT) over the mid-to-high latitudes of Eurasia during 1948–2014. Analyses show that the connection between the spring North Atlantic tripole SST anomaly pattern and the Eurasian SAT anomalies has experienced marked interdecadal shifts around the early 1970s and mid-1990s. The connection is strong during 1954–72 and 1996–2014 but weak during 1973–91. A diagnosis indicates that interdecadal changes in the connection between the North Atlantic SST and Eurasian SAT variations are associated with changes in atmospheric circulation anomalies over Eurasia induced by the North Atlantic tripole SST anomaly pattern. Further analyses suggest that changes in atmospheric circulation anomalies over Eurasia are related to changes in the position of atmospheric heating anomalies over the North Atlantic, which may be due to the change in mean SST. Marked atmospheric heating anomalies appear over the tropical western North Atlantic during 1954–72 and 1996–2014 but over the subtropical central-eastern North Atlantic during 1973–91. Barotropic model experiments confirm that different background flows may also contribute to changes in anomalous atmospheric circulation over Eurasia.

1. Introduction

Surface air temperature (SAT) is an important variable for the climate variability. Changes in the SAT over Eurasia exert pronounced impacts on the economy, society, and people's daily lives. For instance, summer crop yield in northeastern China is significantly influenced by local surface temperature changes (e.g., Sun et al. 1983; Yao 1995). A low summer temperature in northeastern China may significantly reduce the regional crop yield. The extremely high temperatures over Europe in the summer of 2003 resulted in extensive wildfires and substantial economic loss over many parts of Europe (Beniston 2004; Stott et al. 2004). In addition, changes in the SAT over Eurasia during spring and summer may affect the Asian summer monsoon activity via modulating the thermal differences between the land and the surrounding seas (e.g., Liu and Yanai 2001; D'Arrigo et al. 2006). Therefore, it is important to improve the understanding of the SAT variability over Eurasia and its factors.

Studies indicated that the SAT variability over Eurasia is significantly influenced by various factors, such as the Arctic Oscillation (AO) (Thompson and Wallace 1998; Gong et al. 2001; Wu and Wang 2002; Ogi et al. 2005; Miyazaki and Yasunari 2008; Chen et al. 2013), the North Atlantic Oscillation (NAO) (Hurrell and van Loon 1997; Sun et al. 2008; Yuan and Sun 2009; Zveryaev and Gulev 2009), Eurasian snow cover (Ye et al. 2015; Chen et al. 2016; Wu and Chen 2016), and El Niño–Southern Oscillation (ENSO) (Wang et al. 2000; Zhou et al. 2007; Graf and Zanchettin 2012; Cheung et al. 2012; Chen et al. 2013). For example, during the positive (negative) phase of AO or NAO, most regions of Eurasia are covered by positive (negative) SAT anomalies (Thompson and Wallace 1998). Sun et al. (2008) found that SAT variations over central East Asia correlate well with the summer NAO after the late 1970s. An increase (decrease) in snow cover would reduce (increase) the

Corresponding author e-mail: Renguang Wu, renguang@mail.iap.ac.cn

DOI: 10.1175/JCLI-D-16-0477.1

shortwave radiation absorbed by the surface, leading to negative (positive) SAT anomalies (Chen et al. 2016). During El Niño years, a pronounced anticyclonic circulation anomaly appears over the western North Pacific in boreal winter (Wang et al. 2000), leading to an increase in SAT over parts of East Asia as anomalous southwesterly winds to the northwest flank of the anticyclone carry warmer and moister air from the lower latitudes.

Previous studies indicated that the variability of Eurasian SAT in boreal spring is connected with sea surface temperature (SST) anomalies in the North Atlantic (e.g., Wu et al. 2010, 2011; Ye et al. 2015; Chen et al. 2016). These studies showed that the North Atlantic SST anomalies may induce SAT anomalies over Eurasia through anomalous atmospheric wave trains extending from the North Atlantic through Europe to East Asia. Nevertheless, the influence of SST anomalies in the North Atlantic on the SAT variability over the mid-to-high latitudes of Eurasia during boreal spring is not well investigated. In addition, previous studies have demonstrated that the connections of the North Atlantic SST with several climate components are unstable (e.g., Walter and Graf 2002; Wu et al. 2011; Chen et al. 2015a). For example, Walter and Graf (2002) found that the boreal winter North Atlantic SST change is tightly related to the regional atmospheric circulation in the North Atlantic sector during 1969–98, whereas the relationship is weak during 1949–68. Wu et al. (2011) reported that the boreal spring North Atlantic tripole SST anomaly pattern has a strong correlation with the northeastern China summer temperature during the 1980s and 1990s, whereas the connection is weak and insignificant during the 1950s through the mid-1970s. Chen et al. (2015a) showed that the relationship between interannual variations of boreal winter tropical northern Atlantic SST and NAO experienced significant interdecadal changes during the period 1870–2012. According to the above studies, an interesting question is whether the relationship between interannual variations of the boreal spring North Atlantic SST and Eurasian SAT has been subjected to significant changes in the past.

Our analysis reveals several marked interdecadal shifts in the connection between boreal spring North Atlantic SST and Eurasian SAT variations on the interannual time scale during 1948–2014. This study aims to investigate these interdecadal changes and the plausible reasons for these changes. The rest of the paper is organized as follows. Datasets and methods are described in section 2. Section 3 presents observational evidence for the interdecadal changes in the boreal spring North Atlantic SST–Eurasian SAT relationship. Section 4 compares the North Atlantic SST-related anomalies of surface heat fluxes and atmospheric circulation. In section 5, we explore the plausible reasons for the interdecadal changes. Section 6 summarizes the main results of this study.

2. Data and methods

This study uses monthly mean vertical velocity at 500 hPa, winds at 850 and 200 hPa, surface winds at 10 m, surface longwave and shortwave radiation, surface latent and sensible heat fluxes, and total cloud cover (TCC) provided by the National Centers for Environmental Prediction (NCEP)–National Center for Atmospheric Research (NCAR) reanalysis from 1948 to the present (Kalnay et al. 1996). Surface winds, surface heat fluxes, and TCC are on a spectral T62 horizontal resolution Gaussian grid. Vertical velocity at 500 hPa and winds at 850 and 200 hPa are on a 2.5° latitude–longitude grid. The convention for surface heat fluxes is positive for downward flux.

The monthly mean SSTs are obtained from the National Oceanic and Atmospheric Administration (NOAA) Extended Reconstructed SST, version 3b (ERSST.v3b), dataset (Smith et al. 2008). This SST dataset is available from 1854 to the present and has a horizontal resolution of 2° × 2°. This study employs the monthly mean surface air temperature from the University of Delaware (Matsuura and Willmott 2009). This surface air temperature dataset is available from the period 1900–2014 and has a horizontal resolution of 0.5° × 0.5°.

The time period of analysis in this study is 1948–2014, for which all the analyzed variables are available. This study focuses on variations on the interannual time scale. A 9-yr high-pass Lanczos filter (Duchon 1979) has been applied to all monthly mean variables to obtain the component of interannual variations.

We employ the wave activity flux proposed by Takaya and Nakamura (1997, 2001) to depict the propagation of the stationary Rossby waves. As demonstrated by previous studies (Plumb 1985; Takaya and Nakamura 1997, 2001), the wave activity flux is parallel to the local group velocity corresponding to a stationary wave train in the Wentzel–Kramers–Brillouin approximation and is independent of the wave phase. The definition of the wave activity flux is as follows:

$$W = \frac{p}{2|\mathbf{U}|}\begin{Bmatrix} U(v'^2 - \psi' v'_x) + V(-u'v' + \psi' u'_x) \\ U(-u'v' + \psi' u'_x) + V(u'^2 + \psi' u'_y) \\ \dfrac{f_o R_a}{N^2 H_o}[U(v'T' - \psi' T'_x) + V(-u'T' - \psi' T'_y)] \end{Bmatrix},$$

where p, H_o, R_a, T', f_o, and N represent the pressure standardized by 1000 hPa, scale height, gas constant for

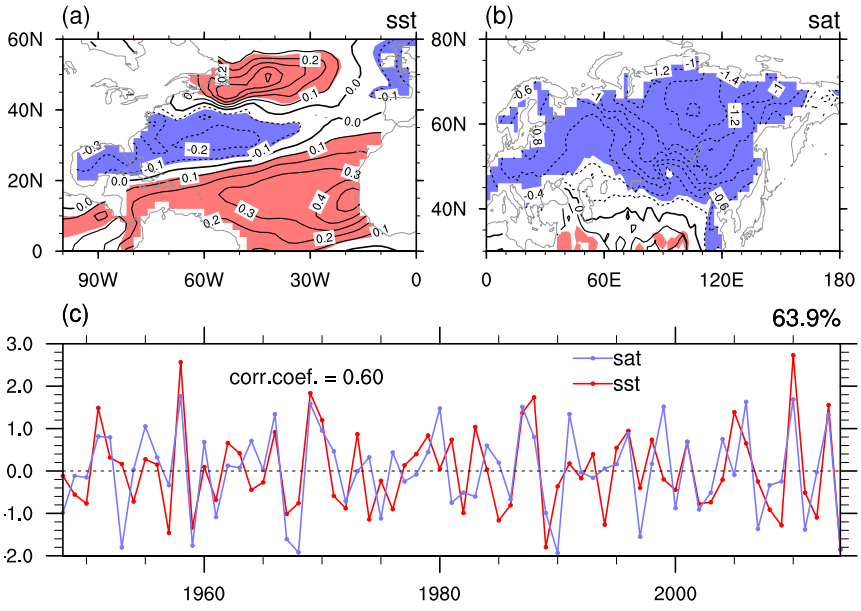

FIG. 1. The first SVD mode between SST in the North Atlantic (0°–60°N, 100°W–20°E) and SAT over the mid-to-high latitudes of Eurasia (Eastern Hemisphere, 30°–80°N) during 1948–2014. (a) MAM SST anomalies (°C) and (b) MAM SAT anomalies (°C) corresponding to the first SVD mode. (c) Standardized SST and SAT expansion coefficient time series corresponding to the first SVD mode. The SST (SAT) anomalies are generated by regressing the SST (SAT) anomaly field onto the standardized SST (SAT) expansion coefficient time series. Shaded regions in (a) and (b) denote anomalies significantly different from zero at the 95% confidence level according to the Student's t test.

dry air, perturbed air temperature, the Coriolis parameter at 45°N, and the Brunt–Väisälä frequency, respectively. Note that p is unitless because it is standardized by 1000 hPa. The variables $\mathbf{V}' = (u', v')$, $\mathbf{U} = (U, V)$, and ψ' denote the perturbed geostrophic winds, mean winds, and perturbed geostrophic streamfunction, respectively. The subscripts x and y denote the derivatives in the zonal and meridional directions, respectively. The climatological mean flow is calculated based on the period 1948–2014. In this study, the perturbations are defined as the anomalies regressed on the North Atlantic tripole SST anomaly index.

3. Interdecadal changes in the North Atlantic SST–Eurasian SAT connection

We employ the singular value decomposition (SVD) analysis to reveal the dominant coupled mode between interannual variations of boreal spring [March–May (MAM)] SST in the North Atlantic and simultaneous spring SAT over the mid-to-high latitudes of Eurasia. The SVD technique can efficiently capture coupled variability related to two fields (e.g., Bretherton et al. 1992; Cherry 1996). Figure 1 displays the first SVD mode of interannual SST anomalies in the North Atlantic (0°–60°N, 100°W–20°E) and interannual SAT anomalies over the mid-to-high latitudes of Eurasia (Eastern Hemisphere, 30°–80°N) in boreal spring during 1948–2014. The first SVD mode accounts for 63.9% of the total squared covariance.

The SST anomaly distribution in the first SVD mode is characterized by a tripole pattern, with significant positive anomalies in the midlatitude and tropical North Atlantic and significant negative anomalies in the subtropical western North Atlantic (Fig. 1a). The SAT anomaly pattern in the first SVD mode is characterized by pronounced negative anomalies over most regions of Eurasia north of 40°N, with two centers located around the Baltic Sea and eastern Siberia, respectively (Fig. 1b). In addition, notable positive SAT anomalies are observed over lower latitudes extending from south of the Caspian Sea eastward to around 100°E (Fig. 1b). The correlation between the expansion coefficient time series of SST and SAT reaches 0.60, significant at the 95% confidence level according to the Student's t test (Fig. 1c). This indicates a coupled variation between the tripole SST anomaly pattern in the North Atlantic and the SAT variations over the mid-to-high latitudes of Eurasia. Note that the coupled variability between the North Atlantic SST and the Eurasian SAT is also

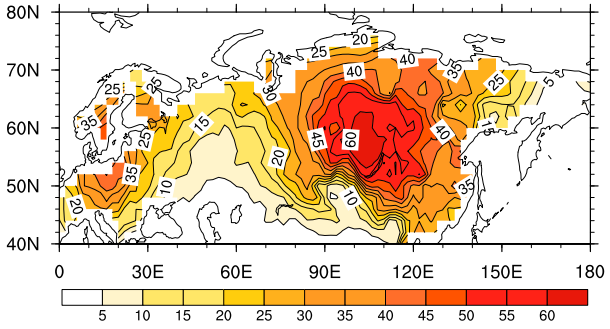

FIG. 2. Spatial distribution of the variance fraction of spring original SAT variability over mid-to-high latitudes of Eurasia accounted for by the first SVD mode for the period of 1948–2014. The contour interval is 5%.

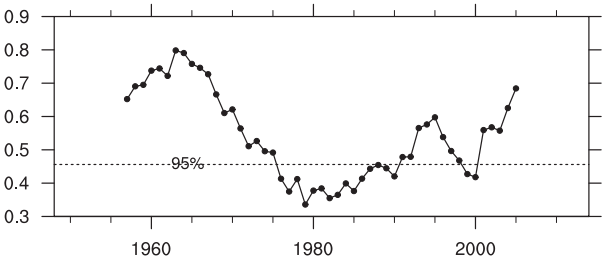

FIG. 3. The 19-yr sliding correlation between the SST and SAT expansion coefficient time series corresponding to the first SVD mode. Note that years are labeled based on the central year of the 19-yr window. The horizontal dashed line indicates the correlation significant at the 95% confidence level according to the Student's *t* test.

observed when the North Atlantic SST leads the Eurasian SAT by about two months (not shown). In the present study, the SST expansion coefficient time series corresponding to the first SVD mode is used as an index for the spring North Atlantic tripole SST anomaly pattern (NATI), and the positive NATI phase corresponds to the SST anomaly pattern shown in Fig. 1a.

The fractional variance of spring SAT variability explained by the first SVD mode (Fig. 2) displays a spatial distribution similar to the loading of the first SVD mode (Fig. 1b). The first SVD mode accounts for above 40% of the total spring SAT variability over central Siberia with the largest value reaching above 60% northwest of Lake Baikal. The fractional variance over western Europe is about 30%. Relatively small fractional variance is observed over eastern Europe, in particular around the Caspian Sea.

To confirm the connection between the North Atlantic tripole SST anomaly and Eurasian SAT variation, we further perform EOF analysis to extract the dominant mode of the North Atlantic SST variability. The distribution of SST anomalies in the North Atlantic revealed by the first EOF mode (not shown) bears a close resemblance to that corresponding to the first SVD mode (Fig. 1a). The correlation coefficient between the principal component time series corresponding to the first EOF mode and the expansion coefficient time series corresponding to the first SVD mode of SST is as high as 0.97.

The relationship between the spring tripole SST anomalies in the North Atlantic and the SAT anomalies over Eurasia is unsteady. This is demonstrated by the sliding correlation between the SST and SAT expansion coefficient time series related to the first SVD mode with a 19-yr window (Fig. 3). Note that similar results are obtained when different lengths of window (e.g., 17, 21, and 23 yr) are employed to calculate the sliding correlations (figures not shown). The correlation is positive and significant at the 95% confidence level before 1975 and after 1991 except for two years, 1999 and 2000 (Fig. 3). In contrast, the correlation is weak and insignificant during 1976–90 (Fig. 3). This indicates that the connection between the spring North Atlantic tripole SST anomaly pattern and the Eurasian SAT variation has experienced interdecadal changes around the early to mid-1970s and 1990s. In the following, we select high- and low-correlation periods to further investigate the interdecadal changes in the spring North Atlantic SST–Eurasian SAT connection. Based on the sliding correlation in Fig. 3, we select two high-correlation periods (i.e., 1954–72 and 1996–2014) and one low-correlation period (i.e., 1973–91). These three periods are selected for comparative analysis because they are not overlapping and the difference of the correlation coefficient between 1954–72 (1996–2014) and 1973–91 is the largest in the analysis period (Fig. 3). According to the Fisher's r–z transformation, the difference of the correlation coefficient between the above neighboring periods is significant at the 95% confidence level.

SAT anomalies related to NATI over Eurasia display notable differences between high- and low-correlation periods. Figure 4 shows spring SAT anomalies obtained by regression on the normalized NATI for 1954–72, 1973–91, and 1996–2014, respectively. During 1954–72, significant negative SAT anomalies appear over western Europe and central-eastern Siberia extending northeastward to the Far East, and pronounced positive anomalies extend from the Arabian Peninsula eastward to southwestern China (Fig. 4a). During 1996–2014, notable negative anomalies are observed over western Europe, similar to those during 1954–72 (Figs. 4a,c). However, the significant negative SAT anomalies over the eastern part of Eurasia shift southwestward compared to those during 1954–72. In addition, pronounced positive SAT anomalies are observed over North Africa

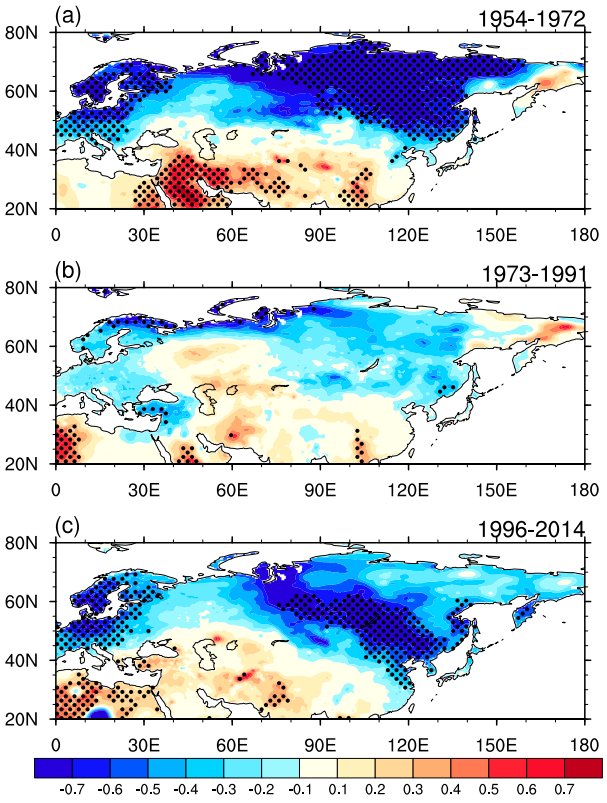

FIG. 4. Anomalies of MAM SAT (°C) obtained by regression on the normalized NATI for (a) 1954–72, (b) 1973–91, and (c) 1996–2014. Stippled regions denote anomalies significantly different from zero at the 95% confidence level according to the Student's *t* test.

during 1996–2014 (Fig. 4c). During 1973–91, the SAT anomalies are weak over most regions of Eurasia except for small regions over the north coast of Europe, North Africa, and the Arabian Peninsula (Fig. 4b). These results confirm that the relationship between the spring North Atlantic tripole SST anomaly pattern and the Eurasian SAT variation is weak and insignificant during the low-correlation period (i.e., 1973–91).

4. North Atlantic SST-related surface heat flux and atmospheric circulation anomalies

In this section, we analyze and compare surface heat flux and atmospheric circulation anomalies associated with the North Atlantic tripole SST anomaly pattern during the three periods to understand the changes in the North Atlantic SST–Eurasian SAT connection. We first analyze surface heat flux and associated surface wind and cloud anomalies to understand surface heat flux anomalies and their contributions to the SAT anomalies. Then, we compare tropospheric atmospheric circulation anomalies to unravel their differences among the three periods. Last, we investigate the reasons for the differences in atmospheric circulation anomalies.

a. Surface heat flux anomalies

During 1954–72, the spatial distribution of surface net heat flux (NHF) anomalies over Eurasia bears a close resemblance to that of SAT anomalies (Figs. 4a and 5a). This indicates that the formation of SAT anomalies is closely related to changes in surface heat fluxes. Significant negative NHF anomalies appear over western Europe and eastern Siberia (Fig. 5a). The sensible heat flux (SHF) is the main contributor to the NHF anomalies in the above regions (Fig. 5j). The longwave radiation (LWR) and latent heat flux (LHF) have an opposite effect (Figs. 5g,m). The shortwave radiation (SWR) has a positive contribution to the NHF anomalies in southern Europe (Fig. 5d). Around the Caspian Sea, positive SWR anomalies are offset by negative LHF and SHF anomalies, leading to small NHF anomalies (Figs. 5a,d,j,m). The negative SHF anomalies over western Europe and eastern Siberia (Fig. 5j) may be explained by northeasterly wind anomalies (Fig. 6a) that bring colder air from higher latitudes, increasing the land–air temperature difference. As the air from the polar oceanic region has a higher humidity compared to that over the land, the land–atmosphere humidity difference is reduced, contributing partly to positive LHF anomalies over the high-latitude regions (Fig. 5m). Negative SWR and positive LWR anomalies over southwestern Europe are related to the increase in TCC (Fig. 7a) that reduces downward SWR and increase downward LWR. The TCC increase is consistent with anomalous lower-level convergence (Fig. 6a) that may lead to anomalous upward motion.

During 1973–91, the NHF anomalies are negative over western Europe, positive over eastern Europe, and negative over most of central-eastern Siberia (Fig. 5b). The spatial distribution of the NHF anomalies is similar to that of the SAT anomalies (Figs. 4b and 5b). However, the NHF anomalies are mostly insignificant, which is consistent with weak SAT anomalies. Negative NHF anomalies over western Europe are attributed to SWR and SHF anomalies (Figs. 5e,k), offset by LWR and LHF anomalies (Figs. 5h,n). Positive NHF anomalies over eastern Europe are contributed by SHF anomalies (Fig. 5k), canceled partly by LHF anomalies (Fig. 5n). Consistently, surface wind anomalies are weak over most of the mid-to-high latitudes of Eurasia except for the Arctic Ocean coast and Far East near Russia (Fig. 6b). Positive TCC anomalies are observed over eastern Europe and east of the Caspian Sea (Fig. 7b), which explain negative SWR and positive LWR anomalies (Figs. 5e,n).

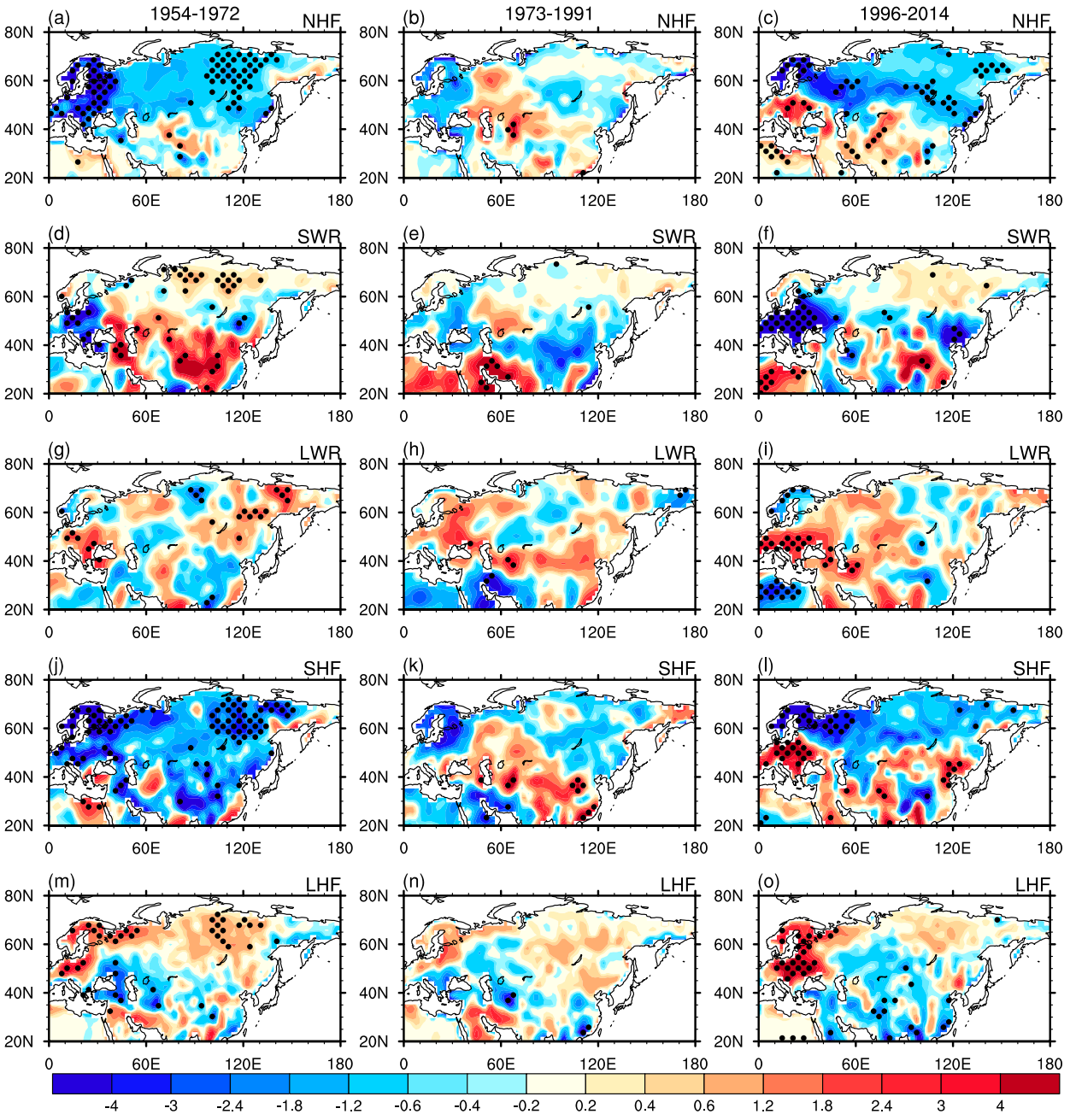

FIG. 5. Anomalies (W m^{-2}) of MAM (a)–(c) NHF, (d)–(f) SWR, (g)–(i) LWR, (j)–(l) SHF, and (m)–(o) LHF obtained by regression on the normalized NATI for (left) 1954–72, (middle) 1973–91, and (right) 1996–2014. Stippled regions denote anomalies significantly different from zero at the 95% confidence level according to the Student's *t* test. Positive (negative) values indicate heat fluxes are downward (upward), which contribute to positive (negative) SAT anomalies.

During 1996–2014, significant negative NHF anomalies extend from western Europe eastward to eastern Siberia (Fig. 5c), contributing to negative SAT anomalies there (Fig. 4c). Negative NHF anomalies over northern part of western Europe are mainly attributed to SHF anomalies (Fig. 5l), whereas LHF anomalies have an opposite effect (Fig. 5o). Changes in SHF and LHF in this region may be related to anomalous northeasterly winds (Fig. 6c). These winds bring colder but wetter air from polar oceanic regions, leading to an increase in land–air temperature difference but a decrease in land–air humidity difference, and thus more upward SHF but less upward LHF (Figs. 5l,o). Negative NHF anomalies over Siberia are primarily due to SHF

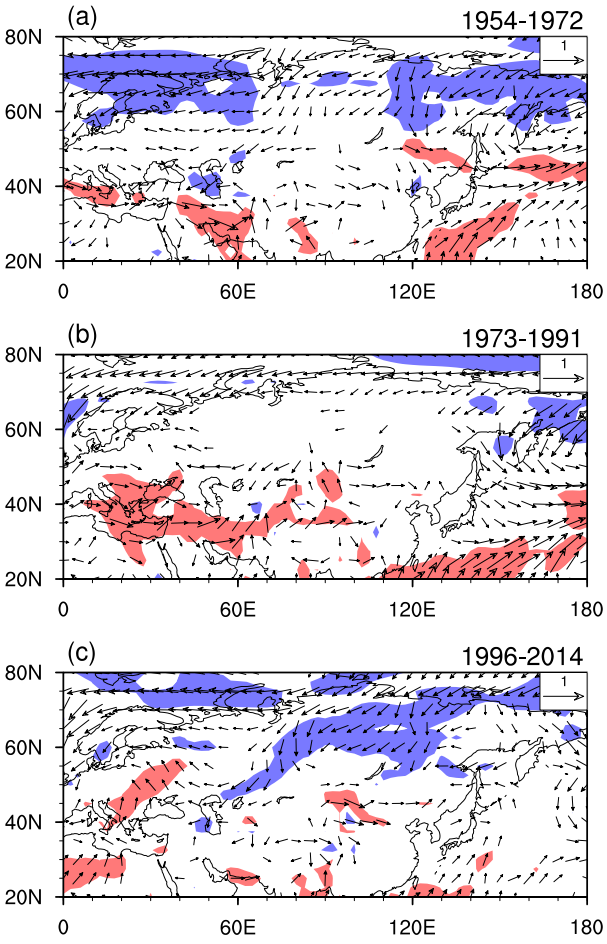

FIG. 6. Anomalies of MAM surface winds (vectors, at 10 m; m s^{-1}) obtained by regression on the normalized NATI for (a) 1954–72, (b) 1973–91, and (c) 1996–2014. The shading indicates that one component of the wind anomaly is significantly different from zero at the 95% confidence level according to the Student's *t* test. Wind anomalies less than 0.1 m s^{-1} are not shown.

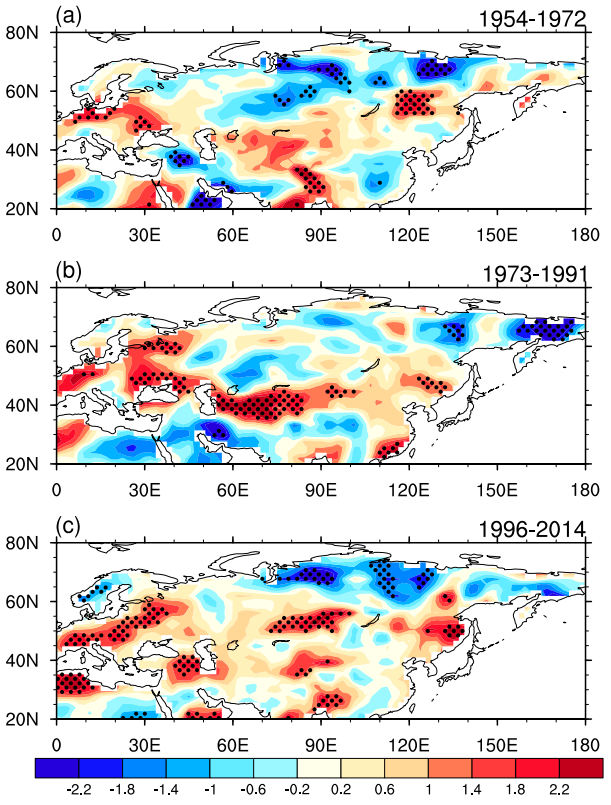

FIG. 7. Anomalies of MAM total cloud cover (%) obtained by regression on the normalized NATI for (a) 1954–72, (b) 1973–91, and (c) 1996–2014. Stippled regions denote anomalies significantly different from zero at the 95% confidence level according to the Student's *t* test.

anomalies (Figs. 5c,l). The SHF anomalies in this region can be explained by anomalous northeasterly winds that bring colder air from higher latitudes (Fig. 6c). To the southeast of Lake Baikal, negative NHF anomalies are contributed by SWR anomalies (Figs. 5c,f), which is consistent with more TCC (Fig. 7c).The negative NHF anomalies extending from western Siberia southeastward to northeastern China contribute to the negative SAT anomalies (Figs. 4c and 5c). Over southwestern Europe, positive NHF anomalies are observed, opposite to the SAT anomalies (Figs. 4c and 5c). Thus, the SAT change cannot be explained by surface heat fluxes. In this region, SWR and LWR anomalies have a positive and negative contribution to the NHF anomalies, respectively (Figs. 5c,f,i). Changes in SWR and LWR in this region are attributed to an anomalous cyclone (Fig. 6c), which increases the TCC (Fig. 7c). The LHF and SHF anomalies are positive in this region (Figs. 5l,o). This is likely associated with anomalous southerly winds (Fig. 6c) that bring warmer and wetter air from lower latitudes, reducing the land–air temperature and humidity difference. The positive LWR, LHF, and SHF anomalies together overcome the negative SWR anomalies, leading to positive NHF anomalies.

We have calculated the different terms of horizontal temperature advection (not shown). Results confirm that the advection of mean temperature by anomalous meridional winds plays an important role in the formation of negative SAT anomalies over the mid-to-high latitudes of Eurasia during 1954–72 and 1996–2014 (Figs. 4a,c). In contrast, during 1973–91, the advection due to anomalous meridional winds is weak over most of the mid-to-high latitudes of Eurasia, which explain weak SAT anomalies there (Fig. 4b).

The above analyses indicate that changes in surface heat fluxes have a large contribution to the formations of SAT anomalies over most of mid-to-high-latitude Eurasia. One exception is southern Europe during

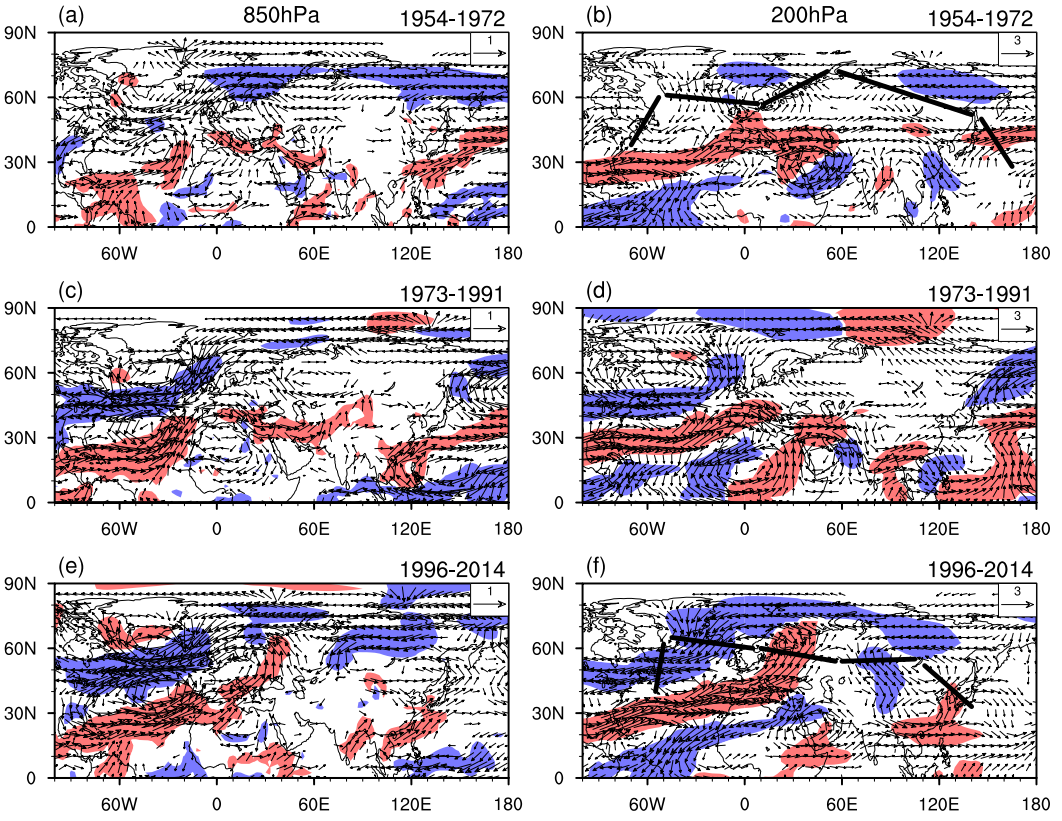

FIG. 8. Anomalies of MAM winds (m s^{-1}) at (left) 850 and (right) 200 hPa obtained by regression on the normalized NATI for (a),(b) 1954–72, (c),(d) 1973–91, and (e),(f) 1996–2014. The shading indicates that one component of the wind anomaly is significantly different from zero at the 95% confidence level according to the Student's *t* test. Wind anomalies less than 0.15 (0.25) m s^{-1} at 850 (200) hPa are not shown. The thick black lines in (b) and (f) indicate atmospheric wave trains from the North Atlantic to Eurasia.

1996–2014. Furthermore, changes in surface heat fluxes are mainly resulted from atmospheric circulation changes. Therefore, atmospheric circulation changes play an important role in connecting the North Atlantic tripole SST anomaly pattern and the Eurasian SAT changes.

b. Atmospheric circulation anomalies

Wind anomalies at 850 and 200 hPa bear some resemblance to each other over mid-to-high latitudes of Eurasia during the three periods (Fig. 8), indicating a barotropic vertical structure. A north–south dipole sea level pressure (SLP) anomaly pattern appears over the North Atlantic during all three periods, with anomalous cyclone and anticyclone around 30° and 60°N, respectively. This dipole SLP anomaly pattern features a typical negative phase of NAO (e.g., Walker and Bliss 1932; Hurrell 1995; Hurrell and van Loon 1997). The correlation coefficient between the spring NAO index and the NATI reaches 0.53 during 1948–2014, significant at the 95% confidence level according to the Student's *t* test. Note that the NAO index employed in this study, which was derived from the Climate Data Guide web page of the University Corporation for Atmospheric Research (UCAR) (https://climatedataguide.ucar.edu/climate-data/hurrell-north-atlantic-oscillation-nao-index-stationbased), was defined as the difference of standardized SLP anomalies between Lisbon, Portugal, and Stykkishólmur and Reykjavik, Iceland (Hurrell 1995). We have calculated the SAT anomalies over Eurasia related to spring NAO index during the three periods (not shown). Significant SAT anomalies in association with the spring NAO index are mainly located over northern Europe during 1954–72 and 1996–2014. By contrast, SAT anomalies related to spring NAO are weak over most of the mid-to-high latitudes of Eurasia during 1973–91, similar to those associated with the spring NATI. The results suggest that the influence of spring NAO on the SAT anomalies over the eastern part of Eurasia are generally weak during the three periods except for small patches over East Asia.

Wind anomalies at 200 hPa over the mid-to-high latitudes of Eurasia display notable differences among the

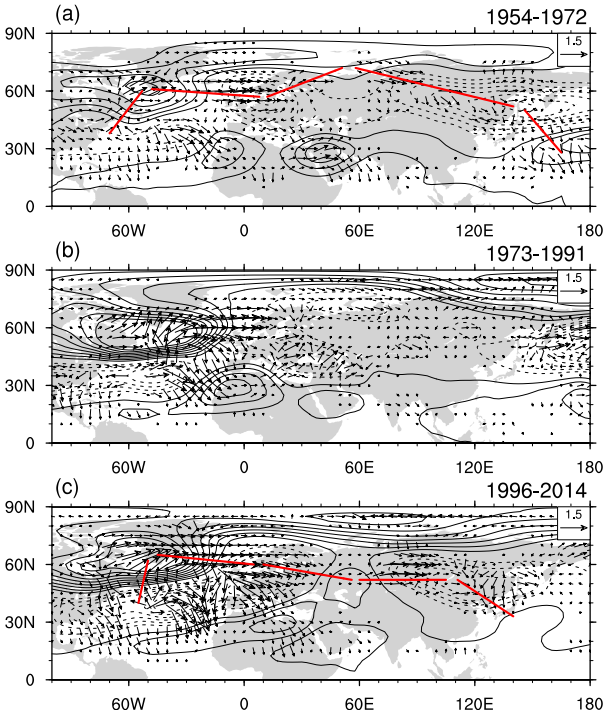

FIG. 9. Anomalies of 500-hPa geopotential height (contours; m) and wave activity flux (vectors; $m^2 s^{-2}$) in MAM obtained by regression on the normalized NATI for (a) 1954–72, (b) 1973–91, and (c) 1996–2014. Anomalies of wave activity flux less than 0.1 $m^2 s^{-2}$ in both directions are not shown. Contour interval for geopotential height is 3 m, and zero contours are omitted. The thick red lines in (a) and (c) are the same as the thick black lines shown in Figs. 8b and 8f, respectively, indicating atmospheric wave trains over the North Atlantic through Eurasia.

three periods. During 1954–72, a wave train is observed from the western North Atlantic, going first northeastward to midlatitude Eurasia around 60°N, next eastward to central Eurasia around 60°E, and then southeastward to East Asia and the North Pacific (Fig. 8b). During 1973–91, there is no clear wave train over the mid-to-high latitudes of Eurasia (Fig. 8d). This explains the weak connection between the North Atlantic SST and the mid-to-high-latitude Eurasian SAT variations. During 1996–2014, the pathway of the atmospheric wave trains from the North Atlantic to Eurasia bear some resemblances to those during 1954–72 but located more southward during 1996–2014 (Figs. 8b,f).

The above-mentioned anomalous wave trains over the North Atlantic through Eurasia during the three periods can also be captured by anomalies of 500-hPa geopotential height and wave activity fluxes (Fig. 9). A wave train is observed over the North Atlantic through Eurasia during both 1954–72 and 1996–2014 (Figs. 9a,c). In comparison, wave activity flux anomalies over mid-to-high-latitude Eurasia are relatively weaker and located at higher latitudes during 1954–72 than during 1996–2014. There is no clear wave train over Eurasia during 1973–91 (Fig. 9b). These are generally consistent with those shown in Fig. 8.

The above results indicate that anomalous atmospheric wave trains from the North Atlantic to Eurasia play an important role in the formation of atmospheric circulation anomalies related to the spring NATI during 1954–72 and 1996–2014, which further lead to pronounced SAT anomalies over Eurasia. By contrast, during 1973–91, the lack of clear atmospheric wave trains over the Eurasian land explains the weak atmospheric circulation and SAT anomalies over Eurasia during this period.

5. Plausible reasons for changes in atmospheric circulation anomalies

An important question is why the spring NATI-related atmospheric circulation anomalies are different among the three periods. To address this question, we examine in detail the spring SST anomalies during the three periods. Spatial patterns of the SST anomalies in the North Atlantic are similar among the three periods, with significant positive anomalies in tropical and midlatitude North Atlantic and pronounced negative anomalies in subtropical western North Atlantic (Fig. 10). The distribution of the North Atlantic SST anomalies is consistent with that in Fig. 1a. The similarity of the SST anomalies in the North Atlantic among the three periods agrees with the similarity of the wind anomalies. This indicates a close association between the North Atlantic SST and wind anomalies. Previous studies have demonstrated that the North Atlantic tripole SST anomaly pattern is tightly connected to atmospheric circulation anomalies related to NAO (Wallace et al. 1990; Czaja and Frankignoul 1999, 2002; Cassou et al. 2004; Wu et al. 2009, 2011). The tripole SST anomaly pattern in the North Atlantic may influence the variability of NAO via the interaction between eddy and mean flow (e.g., Cassou et al. 2004; Hu and Huang 2006a,b). The NAO-related atmospheric circulation anomalies, in turn, may exert an influence on the tripole SST anomaly pattern via changes in surface heat flux and oceanic advection (e.g., Cayan 1992; Marshall et al. 2001; Visbeck et al. 2003).

The SST anomalies in the Pacific and Indian Oceans display notable differences between high- and low-correlation periods. During 1973–91, marked positive SST anomalies appear in the equatorial central-eastern Pacific (Fig. 10b), indicating a connection between ENSO and the North Atlantic tripole SST anomaly pattern during this period. In addition, significant

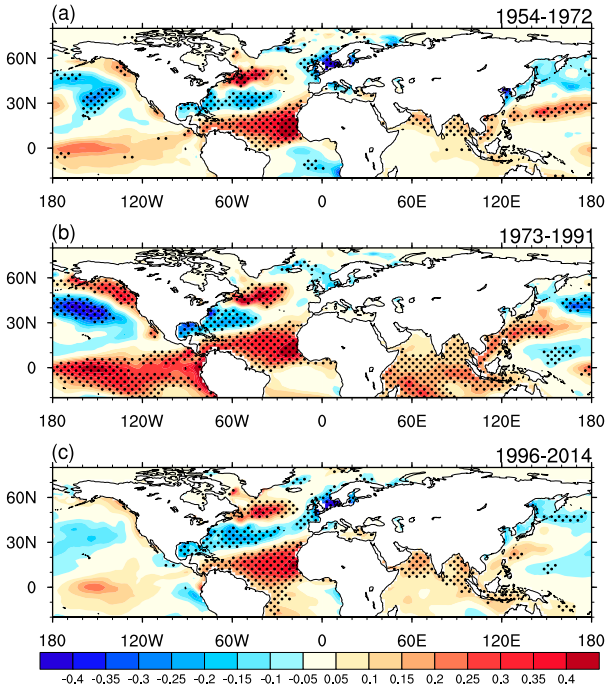

FIG. 10. Anomalies of MAM SST (°C) obtained by regression on the normalized NATI for (a) 1954–72, (b) 1973–91, and (c) 1996–2014. Stippled regions denote anomalies significantly different from zero at the 95% confidence level according to the Student's *t* test.

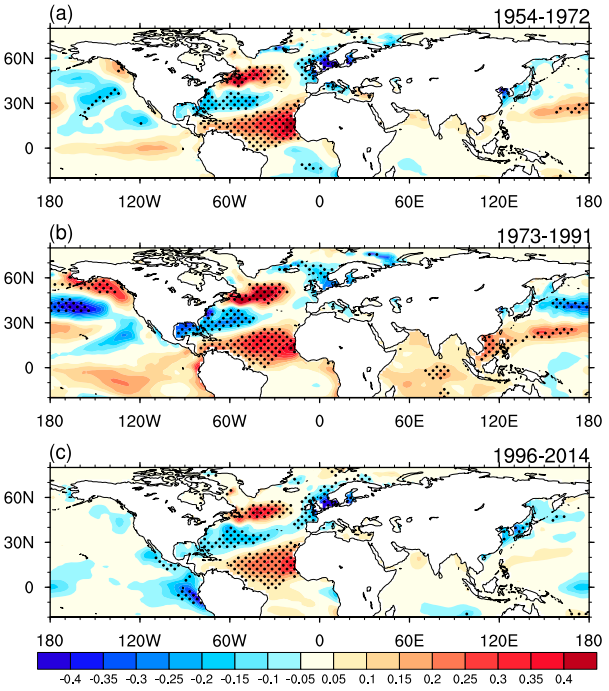

FIG. 11. As in Fig. 10, but with variations in MAM SST and NATI that are linearly correlated with the preceding winter [December–February (DJF) averaged] Niño-3.4 SST index removed by a linear regression.

positive SST anomalies are observed near the west coast of North America and in the tropical Indian Ocean through the South China Sea and subtropical western North Pacific, and pronounced negative anomalies occur in central North Pacific. Formation of the SST anomalies in the abovementioned regions may be partly induced by ENSO. Previous studies have demonstrated that ENSO can influence the SST variability in the North Pacific, the South China Sea, and the Indian and Atlantic Oceans via modulating changes in surface heat fluxes (e.g., Lau and Nath 1996; Klein et al. 1999; Wang et al. 2000; Alexander et al. 2002; Czaja and Frankignoul 2002; Huang et al. 2002, 2004; Wu and Zhang 2010; Wu and Kirtman 2011). In contrast, the SST anomalies in the equatorial central-eastern Pacific and the extratropical North Pacific are weak and the positive SST anomalies in the Indian Ocean are confined to the northern part during 1954–72 and 1996–2014 (Figs. 10a,c).

Can the different SST anomalies in the tropical Pacific explain the difference in atmospheric circulation anomalies over Eurasia among the three periods? To answer this question, we remove the component of spring SST and NATI variations that is associated with ENSO by a linear regression with respect to the preceding winter Niño-3.4 SST index, which is the area-mean SST anomalies averaged over the region of 5°S–5°N, 170°–120°W. The Niño-3.4 SST anomaly is generally used to represent the ENSO variability in previous studies (e.g., Deser et al. 2012; Chen et al. 2014, 2015b). Then, we recalculate the SST anomalies regressed on the normalized NATI for the three periods. The SST tripole anomaly pattern is still present in the North Atlantic during the three periods (Fig. 11). This indicates that the tripole SST anomaly pattern can occur independent of ENSO, consistent with Wu et al. (2011). In addition, we have examined the NATI-associated anomalies of SAT and atmospheric winds over Eurasia after removing the variations related to ENSO. It turns out that the SAT and wind anomalies change little (figures not shown). The results indicate that the ENSO influence cannot explain the interdecadal changes in the NATI-related atmospheric circulation anomalies over the North Atlantic and Eurasia.

Note that the spatial distributions of SST anomalies in the North Pacific associated with the spring NATI during 1973–91 bear some resemblance to those related to the positive phase of the Pacific decadal oscillation (PDO), the leading EOF mode of monthly SST anomalies over the extratropical North Pacific after the global mean SST signal has been removed (Mantua et al. 1997). One question is whether PDO contributes to the

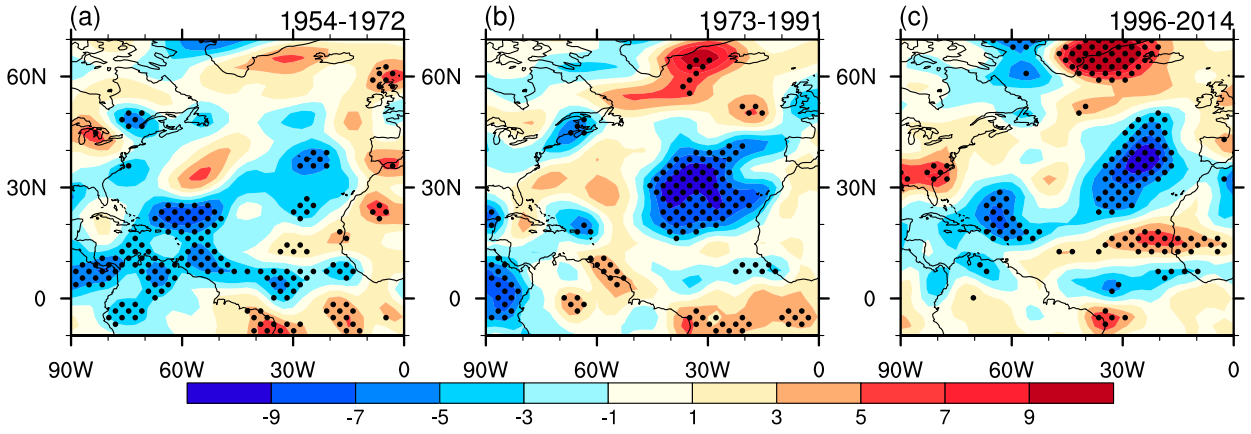

FIG. 12. Anomalies of MAM vertical pressure velocity at 500 hPa (Pa s^{-1}) obtained by regression on the normalized NATI for (a) 1954–72, (b) 1973–91, and (c) 1996–2014. Stippled regions denote anomalies significantly different from zero at the 95% confidence level according to the Student's *t* test.

interdecadal change in the connection between the spring North Atlantic SST and Eurasian SAT variability. To address this issue, we have compared the spring (March–May averaged) PDO index (not shown) with the 19-yr sliding correlation between the North Atlantic SST and Eurasian SAT. Note that the PDO index employed in this paper is derived from the Joint Institute for the Study of the Atmosphere and Ocean available at their website from 1900 to the present (http://jisao.washington.edu/pdo/PDO.latest). It is found that the relationship between the North Atlantic SST and Eurasian SAT tends to be weak (strong) when PDO is in its positive (negative) phase (not shown). The correlation coefficient between the 19-yr running mean of the PDO index and the time series of the 19-yr sliding correlation shown in Fig. 3 reaches −0.74 during the whole analyzed period. This indicates that spring PDO may play a role in the interdecadal change in the relationship between the North Atlantic SST and Eurasian SAT. The mechanism responsible for the influence of spring PDO on the connection between spring North Atlantic SST and Eurasian SAT remains to be investigated.

As demonstrated by previous studies (e.g., Wu et al. 2009, 2010; Chen et al. 2016), SST anomalies in the North Atlantic may exert pronounced influences on atmospheric circulation changes over Eurasia via modulating atmospheric heating. Figure 12 displays anomalies of vertical velocity at 500 hPa obtained by regression on the normalized NATI during 1954–72, 1973–91, and 1996–2014. Substantial differences in the 500-hPa vertical pressure velocity anomalies are observed over the North Atlantic between the high- and low-correlation periods. During 1954–72 and 1996–2014, pronounced upward motion anomalies occur over tropical western North Atlantic (Figs. 12a,c), which may be induced by local positive SST anomalies (Figs. 10a,c). This is supported by anomalous lower-level convergence and upper-level anticyclone (Figs. 8a,b,e,f). Wu et al. (2011) have demonstrated that spring atmospheric heating (indicated by upward motion) over the tropical western North Atlantic can induce an atmospheric wave train extending from the North Atlantic eastward to Eurasia. This indicates that the formation of the wave trains during 1954–72 and 1996–2014 may be partly related to the atmospheric heating anomalies over the tropical western North Atlantic. In contrast, during 1973–91, significant upward motion anomalies appear over the subtropical eastern North Pacific (Fig. 12b). Upward motion anomalies over the tropical western North Atlantic are weak and insignificant during 1973–91. The notable differences in the upward motion anomalies over the North Atlantic between the high- and low-correlation periods imply that the spatial patterns of atmospheric circulation anomalies over the North Atlantic and Eurasia may be sensitive to the location of atmospheric heating, consistent with Chen et al. (2016).

Given the fact that the SST anomaly pattern in the North Atlantic is similar among the three periods (Figs. 10 and 11), why do vertical velocity anomalies over the North Atlantic Ocean display notable differences between high- and low-correlation periods? The atmospheric response to SST anomalies may be dependent upon the mean state. Given the same positive SST anomalies, induced upward motion anomalies would be larger under a higher mean SST because of the nonlinear dependence of atmospheric heating on mean temperature. To address the above issue, we show in Fig. 13 mean SST difference between high- and low-correlation periods. Note that long-term linear trends of SST have been removed by a regression in constructing

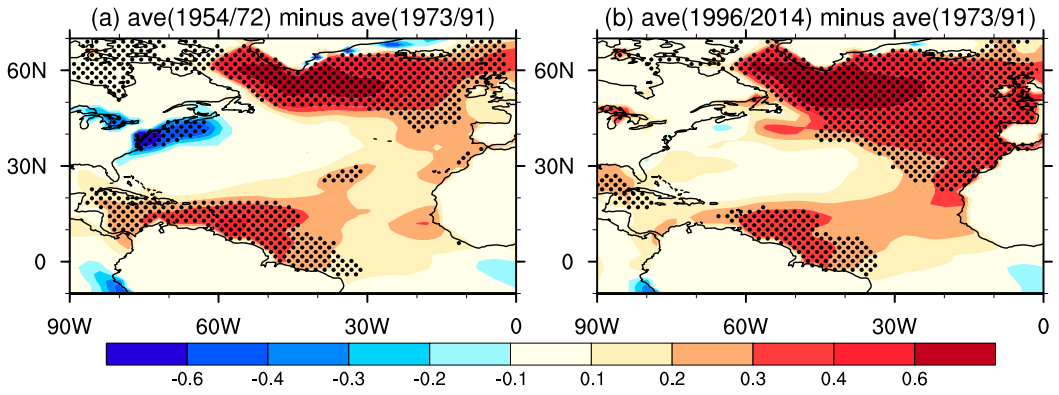

FIG. 13. Difference of mean SST (°C) (a) between1954–72 and 1973–91 and (b) between 1996–2014 and 1973–91. Stippled areas denote the regions where the difference is significant at the 95% confidence level. The long-term linear trend has been removed when constructing the difference.

the difference maps. From Fig. 13, the mean SST during 1954–72 and 1996–2014 is significantly higher than that during 1973–91 by about 0.3°–0.4°C in the tropical and midlatitude North Atlantic (Figs. 13a,b). This suggests that differences in vertical velocity anomalies over the North Atlantic between high- (1954–72 and 1996–2014) and low- (1973–91) correlation periods may be related to the differences in mean SST.

The mean atmospheric circulation change may also play a role in contributing to the differences in anomalous circulation over the North Atlantic and Eurasia. Previous studies have demonstrated that the synoptic eddy forcing, which is an important factor in maintaining the variability of low-frequency flow over the midlatitudes, is highly sensitive to the change in the background flow (Lau and Nath 1991; Peng and Whitaker 1999; Kug and Jin 2009; Zuo et al. 2013). Figure 14 displays differences in mean 200-hPa zonal winds between high- and low-correlation periods. Climatological mean 200-hPa zonal winds are also presented in Fig. 14 for comparison. A subtropical jet extends eastward along 30°N from North Africa to East Asia (Fig. 14) with two centers over west and East Asia, respectively, consistent with previous studies (e.g., Du et al. 2016; Hong and Lu 2016). The mean zonal winds at 200 hPa over Eurasia between 40° and 60°N are stronger during 1954–72 and 1996–2014 than during 1973–91. Significant negative differences are observed over subtropical East Asia around the jet stream center or to the north of the jet stream axis between high- and low-correlation periods (Fig. 14). Positive differences are observed around the center of the subtropical jet stream axis over North Africa (Fig. 14). Furthermore, mean zonal winds over the tropics and high latitudes of the North Atlantic (subtropical North Atlantic) during 1954–72 and 1996–2014 are significantly weaker (stronger) than those during 1973–91. In particular, large positive differences occur to the north of the subtropical North Atlantic jet stream axis (Fig. 14). This implies a significant northward shift of the subtropical North Atlantic jet stream during the high-correlation periods. Hong and Lu (2016) reported that the spatial pattern of atmospheric wave train over Eurasia is significantly impacted by the meridional displacement of the subtropical jet over Eurasia. The above discussion implies that changes in climatological mean winds over the North Atlantic and Europe may also partly contribute to the differences in atmospheric circulation anomalies in association with NATI. Nevertheless, the mechanisms that are

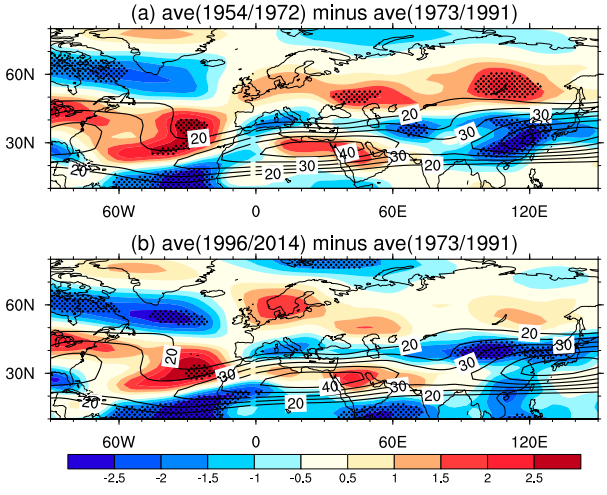

FIG. 14. Difference of mean zonal wind (shading; $m\,s^{-1}$) at 200 hPa (a) between1954–72 and 1973–91 and (b) between 1996–2014 and 1973–91. Stippled areas denote the regions where the difference is significant at the 95% confidence level. Contours represent climatological mean MAM zonal winds at 200 hPa during the period 1948–2014. The long-term linear trend has been removed when constructing the difference.

responsible for the contribution of mean circulation changes to the differences in atmospheric circulation anomalies related to NATI among the three periods remain to be investigated.

In the following, we perform experiments with a barotropic model to confirm the roles of the background circulation and the position of anomalous atmospheric heating in the spatial distribution of atmospheric circulation anomalies over the North Atlantic and Eurasia. As indicated by Sardeshmukh and Hoskins (1988), the barotropic model is able to efficiently capture the essential dynamics of atmospheric anomalies in response to convective heating. The barotropic model used in the present study is spectral, which has the truncation at rhomboidal wavenumber 40. We first perform three pairs of experiments. In each pair, one experiment is forced by spring climatological mean divergence and the other by spring climatological mean divergence plus prescribed divergence anomaly over the given region with a maximum intensity of $7 \times 10^{-6}\,s^{-1}$. In the three pairs, the spring climatological mean divergences are based on periods 1954–72, 1973–91, and 1996–2014, respectively. The locations of specified divergence anomaly are determined according to the upward motion anomaly over the tropical and subtropical North Atlantic in the above three periods, respectively (Fig. 12). In the first and third pairs, the center of the prescribed divergence anomaly is at 12°N, 65°W and 15°N, 65°W, respectively. In the second pair, the center of the prescribed divergence anomaly is at 30°N, 30°W. The barotropic model is integrated for 40 days in all the experiments. The difference between the two experiments in each pair (i.e., imposed spring climatological mean divergence plus prescribed divergence anomaly minus imposed spring climatological mean divergence) is considered as the atmospheric response to imposed divergence anomaly.

Figures 15a–c display the model response for the three periods, respectively, averaged over model days 31–40 with red solid contours indicating the prescribed divergence anomaly. Atmospheric circulation responses based on the barotropic model experiments bear a close resemblance to those in observations. In Fig. 15a, a wave train is observed from the subtropical western North Atlantic, going first northeastward across western Europe to high latitudes of central Eurasia and then southeastward to East Asia and the North Pacific. This is generally consistent with the results from the observations for 1954–72 (Figs. 8a,b). In particular, anomalous cyclones over western Europe and East Asia and anomalous anticyclone over central Eurasia around 60°E are captured by the barotropic model simulation during 1954–72 (Fig. 15a). In Fig. 15b, no clear wave train is observed over mid-to-high latitudes of Eurasia for 1973–91, consistent with the results in Figs. 8c,d. In Fig. 15c, a clear wave train appears over the North Atlantic through northern Europe to East Asia, which is generally in agreement with that in Figs. 8e,f. The above results confirm that spatial distributions of atmospheric circulation anomalies over the North Atlantic and Eurasia are closely related to the background circulation and the position of the convective heating over the North Atlantic.

It should be mentioned that there is a slight difference in the location of anomalous atmospheric wave trains over Eurasia between the barotropic model and observations. For example, the anomalous anticyclone over central Eurasia during 1954–72 is located slightly northward in the barotropic model compared to that in the observations. The anomalous anticyclone during 1996–2014 over the high latitudes of Eurasia is located more northeastward in the barotropic model simulation. These inconsistencies may imply that other processes (such as a baroclinic process and land–atmosphere interaction) may also be important in the formation of the atmospheric circulation anomalies, which remain to be explored.

We perform another three pairs of experiments to examine the relative importance of the background circulation and the position of anomalous atmospheric heating to the formation of atmospheric circulation anomalies during the three periods. The prescribed spring climatological mean divergences are the same as those in Figs. 15a–c, based on periods 1954–72, 1973–91, and 1996–2014, respectively, but we change the location of the center of the prescribed divergence anomaly. The results are shown in Figs. 15d–f. The difference in the response between these two pairs indicates the impact of the change in the position of anomalous atmospheric heating. In addition, as the same divergence anomaly is prescribed in Figs. 15c and 15e (Figs. 15b and 15f), the difference in the response between these two pairs implies the impact of mean circulation change. In Fig. 15d, no wave train is simulated from North Atlantic to Eurasia. The difference between Figs. 15a and 15d indicates that the formation of atmospheric circulation anomalies over Eurasia during 1954–72 is sensitive to the location of the atmospheric heating over the North Atlantic. Previous studies have demonstrated that the influence of the summer North Atlantic tripole SST anomaly on the East Asian summer monsoon is highly dependent on the meridional position of the atmospheric heating related to the tripole SST anomaly (e.g., Zuo et al. 2013). During 1996–2014, an atmospheric wave train is simulated over the mid-to-high latitudes of Eurasia when the divergence anomaly is prescribed around 30°N, 30°W

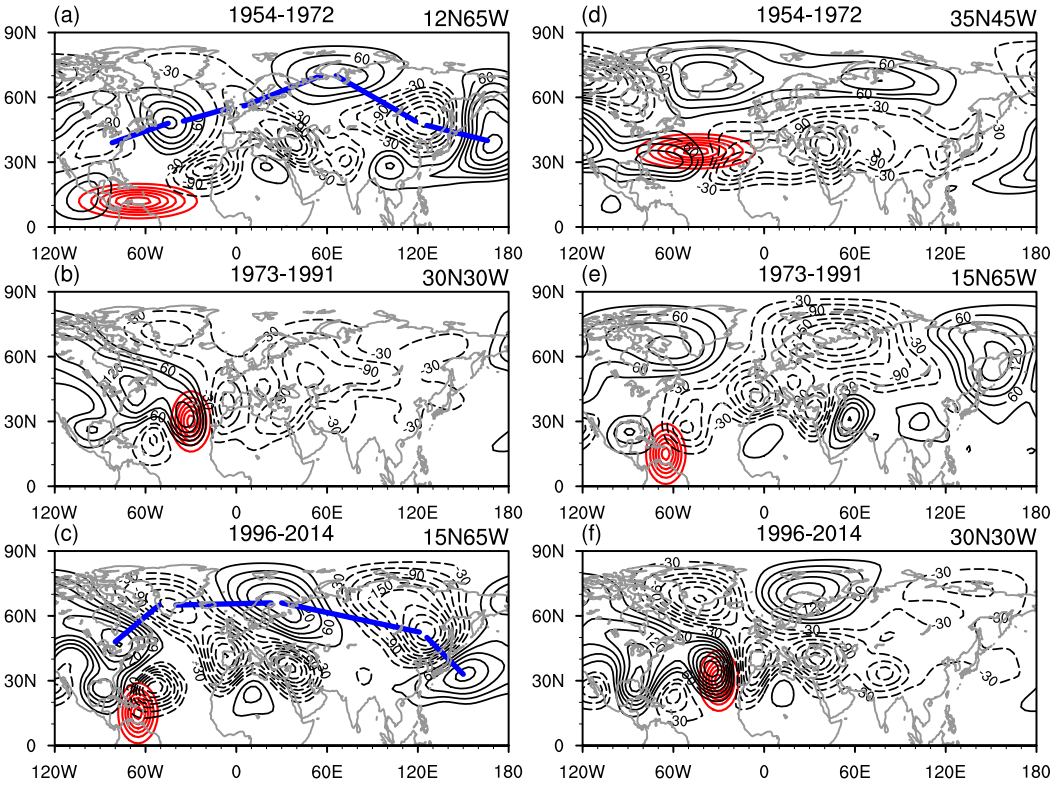

FIG. 15. Barotropic model height perturbation (black contours, with contour interval of 30 m) averaged over days 31–40 in response to imposed idealized divergence anomaly (red contours, with contour interval of $10^{-6}\,s^{-1}$, and zero contour is omitted) over the tropical western Atlantic for (a) 1954–72 (center at 12°N, 65°W), (c) 1996–2014 (center at 15°N, 65°W), and (e) 1973–91 (center at 15°N, 65°W) and over the subtropical North Atlantic for (b) 1973–91 (center at 30°N, 30°W), (d) 1954–72 (center at 35°N, 45°W), and (f) 1996–2014 (center at 30°N, 30°W). Note that the spatial distribution of the imposed divergence anomaly over the tropical western Atlantic in (a) is different from that in (c) and (e), which are related to the spatial distribution of 500-hPa vertical pressure velocity shown in Fig. 12. The thick blue lines in (a) and (c) indicate atmospheric wave trains over the North Atlantic through Eurasia.

(Fig. 15f). Compared to Fig. 15c, the wave train is located slightly northward. In particular, the anomalous cyclone around 120°E is weaker and shifts northward to the Far East. The atmospheric response during 1973–91 in Fig. 15e is featured by a dipole anomaly pattern over Eurasia, with an anomalous anticyclone over eastern Eurasia and an anomalous cyclone over western Eurasia. This is different from that shown in Fig. 15c. The above results suggest that both the background circulation and location of anomalous atmospheric heating are important for atmospheric circulation anomalies over Eurasia during 1973–91 and 1996–2014.

6. Summary

The present study investigates interdecadal changes in the connection between interannual variations of SST in the North Atlantic and SAT over the mid-to-high latitudes of Eurasia during 1948–2014. An analysis using the SVD technique reveals that the Eurasian SAT variations are coupled to the North Atlantic tripole SST anomaly pattern. However, the connection between the North Atlantic tripole SST anomaly pattern and the Eurasian SAT variations is unsteady and has experienced interdecadal shifts around the early 1970s and mid-1990s. The relationship between the North Atlantic tripole SST anomaly pattern and Eurasian SAT variations is strong and statistically significant before the early 1970s and after the mid-1990s, whereas the connection is weak between the mid-1970s and early 1990s. During 1954–72, corresponding to the positive phase of the tripole SST anomaly pattern, with positive anomalies in the tropical and midlatitude North Atlantic and negative anomalies in the subtropical western North Atlantic, pronounced negative SAT anomalies appear over western Europe and the northeastern part of Eurasia, and marked positive SAT anomalies extend eastward from the Arabian Peninsula to northwestern

China. Spatial patterns of the SAT anomalies in association with the North Atlantic tripole SST anomaly pattern during 1996–2014 bear some resemblance to those during 1954–72, but with negative anomalies over the northeastern part of Eurasia shifting southwestward. In contrast, SAT anomalies are weak and insignificant over most regions of Eurasia during 1973–91.

A diagnosis of surface heat fluxes indicates that the formations of the SAT anomalies during the three periods are tightly connected to the changes in surface heat fluxes. A large decrease in downward net surface heat flux is observed over large parts of Eurasia during 1954–72 and 1996–2014, contributing to negative SAT anomalies there. In contrast, changes in net surface heat flux are weak over most parts of Eurasia during 1973–91, consistent with small SAT anomalies.

Atmospheric circulation changes play an important role in forming surface heat fluxes anomalies mainly through wind-induced surface sensible heat flux change and cloud-induced surface radiation change. Notable changes are identified in the atmospheric circulation anomalies over the North Atlantic through the mid-to-high-latitude Eurasia. One wave train appears to exist during 1954–72 over the high-latitudes of Eurasia. There is no clear wave train during 1973–91. One wave train is observed over the midlatitudes of Eurasia during 1996–2014.

Further analyses suggest that the differences in atmospheric circulation anomalies among the three periods are closely related to the change in the position of atmospheric heating anomalies over the North Atlantic and the change in the background circulation. Pronounced upward motion anomalies are observed over the tropical western North Atlantic during 1954–72 and 1996–2014. In contrast, significant upward motion anomalies appear over the subtropical central-eastern Atlantic during 1973–91. Change in the location of significant upward motion anomalies during the three periods is related to the change in mean SST. The mean SST during 1954–72 and 1996–2014 is significantly higher than that during 1973–91 in the tropical North Atlantic. Because of the nonlinearity of dependence of atmospheric heating on mean temperature, a higher mean SST would lead to stronger upward motion anomalies given the same positive SST anomalies over the tropical western North Atlantic. Results from barotropic model experiments confirm that changes in the spatial pattern of anomalous atmospheric circulation over the North Atlantic and Eurasia associated with the North Atlantic tripole SST anomaly pattern are related to the changes in the position of the anomalous convective heating over the North Atlantic and the changes in background circulation.

The present study interpreted changes in the connection between the North Atlantic SST and Eurasian SAT variations from the impacts of location of anomalous heating and mean state. The reasons why spatial patterns of anomalous circulation over the North Atlantic and Eurasia are sensitive to the change in background circulation remain to be explored. In addition to the North Atlantic SST anomalies, other factors may contribute to the Eurasian SAT variations. The interdecadal changes addressed in the present study may be related to the change in the impacts of other factors. Further studies are needed to identify these factors and the changes of their impacts on the Eurasian SAT variations.

Acknowledgments. We thank three anonymous reviewers for their constructive suggestions and comments, which led to a significant improvement in the paper. This study is supported by a National Key Basic Research Program of China Grant (2014CB953902), National Natural Science Foundation of China Grants (41530425, 41275081, 41475081, and 41605050), National Key Research and Development Program of China grant (2016YFA0600603), Young Talent Support Program of the Chinese Meteorological Society (2016–2018), and China Postdoctoral Science Foundation (2015M581151). We also thank Dr. L. Song and Dr. K.-M. Hu for their helpful discussion. (The University of Delaware data were obtained from http://www.esrl.noaa.gov/psd/data/gridded/, NCEP–NCAR reanalysis variables were obtained from ftp://ftp.cdc.noaa.gov/, and ERSST.v3b data were obtained from http://www.esrl.noaa.gov/psd/data/gridded/.)

REFERENCES

Alexander, M. A., I. Bladé, M. Newman, J. R. Lanzante, N.-C. Lau, and J. D. Scott, 2002: The atmospheric bridge: The influence of ENSO teleconnections on air–sea interaction over the global oceans. *J. Climate*, **15**, 2205–2231, doi:10.1175/1520-0442(2002)015<2205:TABTIO>2.0.CO;2.

Beniston, M., 2004: The 2003 heat wave in Europe: A shape of things to come? An analysis based on Swiss climatological data and model simulations. *Geophys. Res. Lett.*, **31**, L02202, doi:10.1029/2003GL018857.

Bretherton, C. S., C. Smith, and J. M. Wallace, 1992: An intercomparison of methods for finding coupled patterns in climate data. *J. Climate*, **5**, 541–560, doi:10.1175/1520-0442(1992)005<0541:AIOMFF>2.0.CO;2.

Cassou, C., C. Deser, L. Terray, J. W. Hurrell, and M. Drévillon, 2004: Summer sea surface temperature conditions in the North Atlantic and their impact upon the atmospheric circulation in early winter. *J. Climate*, **17**, 3349–3363, doi:10.1175/1520-0442(2004)017<3349:SSSTCI>2.0.CO;2.

Cayan, D. R., 1992: Latent and sensible heat flux anomalies over the northern oceans: Driving the sea surface temperature. *J. Phys. Oceanogr.*, **22**, 859–881, doi:10.1175/1520-0485(1992)022<0859:LASHFA>2.0.CO;2.

Chen, S., W. Chen, and K. Wei, 2013: Recent trends in winter temperature extremes in eastern China and their relationship with the Arctic Oscillation and ENSO. *Adv. Atmos. Sci.*, **30**, 1712–1724, doi:10.1007/s00376-013-2296-8.

——, B. Yu, and W. Chen, 2014: An analysis on the physical process of the influence of AO on ENSO. *Climate Dyn.*, **42**, 973–989, doi:10.1007/s00382-012-1654-z.

——, R. Wu, and W. Chen, 2015a: The changing relationship between interannual variations of the North Atlantic Oscillation and northern tropical Atlantic SST. *J. Climate*, **28**, 485–504, doi:10.1175/JCLI-D-14-00422.1.

——, ——, ——, and B. Yu, 2015b: Influence of the November Arctic Oscillation on the subsequent tropical Pacific sea surface temperature. *Int. J. Climatol.*, **35**, 4307–4317, doi:10.1002/joc.4288.

——, ——, and Y. Liu, 2016: Dominant modes of interannual variability in Eurasian surface air temperature during boreal spring. *J. Climate*, **29**, 1109–1125, doi:10.1175/JCLI-D-15-0524.1.

Cherry, S., 1996: Singular value decomposition analysis and canonical correlation analysis. *J. Climate*, **9**, 2003–2009, doi:10.1175/1520-0442(1996)009<2003:SVDAAC>2.0.CO;2.

Cheung, H., W. Zhou, H. Mok, and M. Wu, 2012: Relationship between Ural–Siberian blocking and the East Asian winter monsoon in relation to the Arctic Oscillation and the El Niño–Southern Oscillation. *J. Climate*, **25**, 4242–4257, doi:10.1175/JCLI-D-11-00225.1.

Czaja, A., and C. Frankignoul, 1999: Influence of the North Atlantic SST on the atmospheric circulation. *Geophys. Res. Lett.*, **26**, 2969–2972, doi:10.1029/1999GL900613.

——, and ——, 2002: Observed impact of Atlantic SST anomalies on the North Atlantic Oscillation. *J. Climate*, **15**, 606–623, doi:10.1175/1520-0442(2002)015<0606:OIOASA>2.0.CO;2.

D'Arrigo, R., R. Wilson, and J. Li, 2006: Increased Eurasian-tropical temperature amplitude difference in recent centuries: Implications for the Asian monsoon. *Geophys. Res. Lett.*, **33**, L22706, doi:10.1029/2006GL027507.

Deser, C., and Coauthors, 2012: ENSO and Pacific decadal variability in the Community Climate System Model version 4. *J. Climate*, **25**, 2622–2651, doi:10.1175/JCLI-D-11-00301.1.

Du, Y., T. Li, Z. Xie, and Z. Zhu, 2016: Interannual variability of the Asian subtropical westerly jet in boreal summer and associated with circulation and SST anomalies. *Climate Dyn.*, **46**, 2673–2688, doi:10.1007/s00382-015-2723-x.

Duchon, C. E., 1979: Lanczos filtering in one and two dimensions. *J. Appl. Meteor.*, **18**, 1016–1022, doi:10.1175/1520-0450(1979)018<1016:LFIOAT>2.0.CO;2.

Gong, D. Y., S. W. Wang, and J. H. Zhu, 2001: East Asian winter monsoon and Arctic Oscillation. *Geophys. Res. Lett.*, **28**, 2073–2076, doi:10.1029/2000GL012311.

Graf, H. F., and D. Zanchettin, 2012: Central Pacific El Niño, the "subtropical bridge," and Eurasian climate. *J. Geophys. Res.*, **117**, D01102, doi:10.1029/2011JD016493.

Hong, X., and R. Lu, 2016: The meridional displacement of the summer Asian jet, Silk Road pattern, and tropical SST anomalies. *J. Climate*, **29**, 3753–3766, doi:10.1175/JCLI-D-15-0541.1.

Hu, Z.-Z., and B. Huang, 2006a: Air–sea coupling in the North Atlantic during summer. *Climate Dyn.*, **26**, 441–457, doi:10.1007/s00382-005-0094-4.

——, and ——, 2006b: On the significance of the relationship between the North Atlantic Oscillation in early winter and Atlantic sea surface temperature anomalies. *J. Geophys. Res.*, **111**, D12103, doi:10.1029/2005JD006339.

Huang, B., P. S. Schopf, and Z. Pan, 2002: The ENSO effect on the tropical Atlantic variability: A regionally coupled model study. *Geophys. Res. Lett.*, **29**, 2039, doi:10.1029/2002GL014872.

——, ——, and J. Shukla, 2004: Intrinsic ocean–atmosphere variability of the tropical Atlantic Ocean. *J. Climate*, **17**, 2058–2077, doi:10.1175/1520-0442(2004)017<2058:IOVOTT>2.0.CO;2.

Hurrell, J. W., 1995: Decadal trends in the North Atlantic oscillation. *Science*, **269**, 676–679, doi:10.1126/science.269.5224.676.

——, and H. van Loon, 1997: Decadal variations in climate associated with the North Atlantic Oscillation. *Climatic Change at High Elevation Sites*, H. F. Diaz, M. Beniston, and R. Bradley, Eds., Springer, 69–94.

Kalnay, E., and Coauthors, 1996: The NCEP/NCAR 40-Year Reanalysis Project. *Bull. Amer. Meteor. Soc.*, **77**, 437–471, doi:10.1175/1520-0477(1996)077<0437:TNYRP>2.0.CO;2.

Klein, S. A., B. J. Soden, and N.-C. Lau, 1999: Remote sea surface temperature variations during ENSO: Evidence for a tropical atmospheric bridge. *J. Climate*, **12**, 917–932, doi:10.1175/1520-0442(1999)012<0917:RSSTVD>2.0.CO;2.

Kug, J.-S., and F.-F. Jin, 2009: Left-hand rule for synoptic eddy feedback on low-frequency flow. *Geophys. Res. Lett.*, **36**, L05709, doi:10.1029/2008GL036435.

Lau, N., and M. Nath, 1991: Variability of the baroclinic and barotropic transient eddy forcing associated with monthly changes in the midlatitude storm tracks. *J. Atmos. Sci.*, **48**, 2589–2613, doi:10.1175/1520-0469(1991)048<2589:VOTBAB>2.0.CO;2.

——, and ——, 1996: The role of the "atmospheric bridge" in linking tropical Pacific ENSO events to extratropical SST anomalies. *J. Climate*, **9**, 2036–2057, doi:10.1175/1520-0442(1996)009<2036:TROTBI>2.0.CO;2.

Liu, X., and M. Yanai, 2001: Relationship between the Indian monsoon rainfall and the tropospheric temperature over the Eurasian continent. *Quart. J. Roy. Meteor. Soc.*, **127**, 909–937, doi:10.1002/qj.49712757311.

Mantua, N. J., S. R. Hare, Y. Zhang, J. M. Wallace, and R. C. Francis, 1997: A Pacific interdecadal climate oscillation with impacts on salmon production. *Bull. Amer. Meteor. Soc.*, **78**, 1069–1079, doi:10.1175/1520-0477(1997)078<1069:APICOW>2.0.CO;2.

Marshall, J., and Coauthors, 2001: North Atlantic climate variability: Phenomena, impacts and mechanisms. *Int. J. Climatol.*, **21**, 1863–1898, doi:10.1002/joc.693.

Matsuura, K., and C. J. Willmott, 2009: Terrestrial air temperature: 1900–2008 gridded monthly time series, version 4.01. University of Delaware Dept. of Geography Center for Climatic Research, accessed 6 August 2015. [Available online at http://www.esrl.noaa.gov/psd/data/gridded/data.UDel_AirT_Precip.html.]

Miyazaki, C., and T. Yasunari, 2008: Dominant interannual and decadal variability of winter surface air temperature over Asia and the surrounding oceans. *J. Climate*, **21**, 1371–1386, doi:10.1175/2007JCLI1845.1.

Ogi, M., K. Yamazaki, and Y. Tachibana, 2005: The summer northern annular mode and abnormal summer weather in 2003. *Geophys. Res. Lett.*, **32**, L04706, doi:10.1029/2004GL021528.

Peng, S., and J. S. Whitaker, 1999: Mechanisms determining the atmospheric response to midlatitude SST anomalies. *J. Climate*, **12**, 1393–1408, doi:10.1175/1520-0442(1999)012<1393:MDTART>2.0.CO;2.

Plumb, R. A., 1985: On the three-dimensional propagation of stationary waves. *J. Atmos. Sci.*, **42**, 217–229, doi:10.1175/1520-0469(1985)042<0217:OTTDPO>2.0.CO;2.

Sardeshmukh, P. D., and B. J. Hoskins, 1988: The generation of global rotational flow by steady idealized tropical divergence. *J. Atmos. Sci.*, **45**, 1228–1251, doi:10.1175/1520-0469(1988)045<1228:TGOGRF>2.0.CO;2.

Smith, T. M., R. W. Reynolds, T. C. Peterson, and J. Lawrimore, 2008: Improvements to NOAA's historical merged land–ocean surface temperature analysis (1880–2006). *J. Climate*, **21**, 2283–2296, doi:10.1175/2007JCLI2100.1.

Stott, P. A., D. A. Stone, and M. R. Allen, 2004: Human contribution to the European heatwave of 2003. *Nature*, **432**, 610–614, doi:10.1038/nature03089.

Sun, J. Q., H. J. Wang, and W. Yuan, 2008: Decadal variations of the relationship between the summer North Atlantic Oscillation and middle East Asian air temperature. *J. Geophys. Res.*, **113**, D15107, doi:10.1029/2007JD009626.

Sun, Y.-T., S.-Y. Wang, and Y.-Q. Yang, 1983: Studies on cool summer and crop yield in northeast China (in Chinese). *Acta Meteor. Sin.*, **41**, 313–321.

Takaya, K., and H. Nakamura, 1997: A formulation of a wave-activity flux for stationary Rossby waves on a zonally varying basic flow. *Geophys. Res. Lett.*, **24**, 2985–2988, doi:10.1029/97GL03094.

——, and ——, 2001: A formulation of a phase-independent wave-activity flux for stationary and migratory quasigeostrophic eddies on a zonally varying basic flow. *J. Atmos. Sci.*, **58**, 608–627, doi:10.1175/1520-0469(2001)058<0608:AFOAPI>2.0.CO;2.

Thompson, D. W., and J. M. Wallace, 1998: The Arctic Oscillation signature in the wintertime geopotential height and temperature fields. *Geophys. Res. Lett.*, **25**, 1297–1300, doi:10.1029/98GL00950.

Visbeck, M., E. P. Chassignet, R. G. Curry, T. L. Delworth, R. R. Dickson, and G. Krahmann, 2003: The ocean's response to North Atlantic Oscillation variability. *The North Atlantic Oscillation: Climatic Significance and Environmental Impact*, *Geophys. Monogr.*, Vol. 134, Amer. Geophys. Union, 113–145.

Walker, G. T., and E. Bliss, 1932: World weather V. *Mem. Roy. Meteor. Soc.*, **4**, 53–84.

Wallace, J. M., C. Smith, and Q. Jiang, 1990: Spatial patterns of atmosphere–ocean interaction in the northern winter. *J. Climate*, **3**, 990–998, doi:10.1175/1520-0442(1990)003<0990:SPOAOI>2.0.CO;2.

Walter, K., and H. F. Graf, 2002: On the changing nature of the regional connection between the North Atlantic Oscillation and sea surface temperature. *J. Geophys. Res.*, **107**, 4338, doi:10.1029/2001JD000850.

Wang, B., R. Wu, and X. Fu, 2000: Pacific–East Asian teleconnection: How does ENSO affect East Asian climate? *J. Climate*, **13**, 1517–1536, doi:10.1175/1520-0442(2000)013<1517:PEATHD>2.0.CO;2.

Wu, B., and J. Wang, 2002: Winter Arctic Oscillation, Siberian high and East Asian winter monsoon. *Geophys. Res. Lett.*, **29**, 1897, doi:10.1029/2002GL015373.

Wu, R., and L. Zhang, 2010: Biennial relationship of rainfall variability between Central America and equatorial South America. *Geophys. Res. Lett.*, **37**, L08701, doi:10.1029/2010GL042732.

——, and B. P. Kirtman, 2011: Caribbean Sea rainfall variability during the rainy season and relationship to the equatorial Pacific and tropical Atlantic SST. *Climate Dyn.*, **37**, 1533–1550, doi:10.1007/s00382-010-0927-7.

——, and S. Chen, 2016: Regional change in snow water equivalent–surface air temperature relationship over Eurasia during boreal spring. *Climate Dyn.*, **47**, 2425–2442, doi:10.1007/s00382-015-2972-8.

——, S. Yang, S. Liu, L. Sun, Y. Lian, and Z. Gao, 2010: Changes in the relationship between northeast China summer temperature and ENSO. *J. Geophys. Res.*, **115**, D21107, doi:10.1029/2010JD014422.

——, ——, ——, ——, ——, and ——, 2011: Northeast China summer temperature and North Atlantic SST. *J. Geophys. Res.*, **116**, D16116, doi:10.1029/2011JD015779.

Wu, Z., B. Wang, J. Li, and F. F. Jin, 2009: An empirical seasonal prediction model of the East Asian summer monsoon using ENSO and NAO. *J. Geophys. Res.*, **114**, D18120, doi:10.1029/2009JD011733.

Yao, P.-Z., 1995: The climate features of summer low temperature cold damage in northeast China during recent 40 years (in Chinese). *J. Catastrophology*, **10**, 51–56.

Ye, K., R. Wu, and Y. Liu, 2015: Interdecadal change of Eurasian snow, surface temperature, and atmospheric circulation in the late 1980s. *J. Geophys. Res. Atmos.*, **120**, 2738–2753, doi:10.1002/2015JD023148.

Yuan, W., and J. Q. Sun, 2009: Enhancement of the summer North Atlantic Oscillation influence on Northern Hemisphere air temperature. *Adv. Atmos. Sci.*, **26**, 1209–1214, doi:10.1007/s00376-009-8148-x.

Zhou, W., X. Wang, T. J. Zhou, C. Y. Li, and J. C. L. Chan, 2007: Interdecadal variability of the relationship between the East Asian winter monsoon and ENSO. *Meteor. Atmos. Phys.*, **98**, 283–293, doi:10.1007/s00703-007-0263-6.

Zuo, J., W. Li, C. Sun, L. Xu, and H. Ren, 2013: Impact of the North Atlantic sea surface temperature tripole on the East Asian summer monsoon. *Adv. Atmos. Sci.*, **30**, 1173–1186, doi:10.1007/s00376-012-2125-5.

Zveryaev, I. I., and S. K. Gulev, 2009: Seasonality in secular changes and interannual variability of European air temperature during the twentieth century. *J. Geophys. Res.*, **114**, D02110, doi:10.1029/2008JD010624.